19.2 A Mechanically Flexible Implantable Neural Interface for Computational Imaging and Optogenetic Stimulation over 5.4×5.4mm² FoV

Sajjad Moazeni*[1,2], Eric H. Pollmann*[1], Vivek Boominathan[3], Filipe A. Cardoso[1], Jacob T. Robinson[3], Ashok Veeraraghavan[3], Kenneth L. Shepard[1]

[1]Columbia University, New York, NY
[2]University of Washington, Seattle, WA
[3]Rice University, Houston, TX

*Equally-Credited Authors (ECAs)

The advent of genetically encoded voltage and calcium indicators and optogenetic probes has unlocked unprecedented capabilities, including near-single-action-potential recording and stimulation with cell-type specificity. Optical functional imaging and optogenetics are delegated today primarily to large and expensive microscopes based on free-space optics. Integrating the microscope functionality into an implantable form factor remains an elusive goal. As a first step towards developing such a device, a variety of head-mounted "miniscopes" have been demonstrated [1]. Using conventional lens-based optics, however, these devices consume considerable volume (more than 2cm³) to support field of views (FoVs) of sub-mm². To achieve a truly implantable microscope, a more volume-efficient device is necessary that spans a relatively large cortical area while maintaining a minimally-invasive form factor.

In this paper, we demonstrate a new device ultimately capable of a fully implantable form factor that supports all-optical neural recording and stimulation over a 5.4×5.4mm² FoV at depths up to 200µm in cortex (Layer 2/3 in mouse). This mechanically flexible, implantable brain-surface device, illustrated in Fig. 19.2.1, enables fluorescence imaging in an ultra-thin (<250µm-thick) form factor by exploiting a lens-less computational imaging approach. Device functionality is provided by a die-thinned CMOS integrated circuit consisting of 2D arrays of monolithically integrated single-photon avalanche photodiode (SPAD) detectors and flip-chip bonded micro-LED (µLED) light emitters for both fluorescence excitation and optogenetic stimulation. While the proof-of-concept device is wired, the final embodiment of this device will be interfaced wirelessly, as shown in Fig. 19.2.1.

Lens-less computational imaging is realized with a coded-aperture binary mask [2]. The mask is fabricated by patterning a 100nm-thick chromium layer with 15µm feature sizes onto an optical filter and bonded onto the chip (Fig. 19.2.1). In a lens-based system, the lens collects and focuses light from the scene pixels to the sensor pixels with a one-to-one mapping, but in a computational lens-less system, unfocused light from a single point on the scene is spatially modulated (by the mask) and mapped to multiple sensor pixels. After calibrating the imager, the scene is computationally reconstructed by running an inverse imaging algorithm on the raw capture. The far-field amplitude masking approach employed here does not limit the photon reception angle, leading to higher imaging sensitivity that achieved with near-field approaches [3, 4].

For fluorescence imaging, we employ a long-pass absorption filter to block back-scattered excitation light, which is fabricated in 100µm-thick flexible gelatin and provides 26dB rejection of the 470nm excitation light relative to fluorescence emission at 520nm. This filter accepts wide-angle photons and also acts as the 100µm spacer required to separate the mask from the imager. The filter is laser cut to create openings for two separate 5×5 arrays of blue (470nm) and green (535nm) Cree µLEDs for fluorescence excitation and optogenetic stimulation, respectively.

The imager was designed in a 0.13µm high-voltage CMOS process and is die-thinned by mechanical backside grinding and polishing to less than 20µm so as to be flexible. Figure 19.2.2 depicts the chip block diagram and imaging timing diagram. The imager operates in photon-counting mode with a configurable, sliding time-gate. Gating the sensor provides an addition ~10dB of background rejection from scattered excitation light and also enables a fluorescence life-time imaging (FLIM) mode [5]. In order to reduce power, area, and readout data rate requirements, the imager employs a rolling-shutter which is combined with selective powering of the excitation µLEDs to reduce power and also help to reduce excitation background. The imager is comprised of 5x5 array of macros, each consisting of 16 blocks in a 4×4 configuration. Of these blocks, 14 are 8×8 SPAD arrays, one is for the excitation µLED, and one is for the optogenetic µLED. Each high-swing µLED driver is equipped with ~0.1nF of decoupling capacitance. During the selection of each sub-frame, which consist of a 5×1 macro column, only excitation µLEDs in the given column are activated. The SPAD array blocks are enabled column-wise where each pixel remains active for 1024 excitation pulses of the µLED, and the detected photon counts are stored in shared-row 10-bit counters. Overall, the imager achieves a frame-rate of 125fps with a 40MHz reference clock. The data transmitter (Tx) block serializes the counter values and sends them off-chip to a control FPGA.

Optogenetic stimulation signals have tunable repetition-rates (5-to-40Hz) and pulse-widths (with 0.1ms LSB precision). The optogenetic µLED columns are also time-multiplexed to reduce the peak current and required on-chip decoupling capacitance. The stimulation pattern can be configured by enabling individual µLEDs, each one illuminating ~0.2mm³ brain regions covering the entire FoV.

Micrographs of the chip and major sub-blocks are shown in Fig. 19.2.3. SPADs are implemented with a 7.5µm-diameter active area. Pixels have a 30µm pitch with in-pixel active quench and reset circuitry (AQC) and 5% effective fill-factor (FF). We characterized the spectral response of the SPAD sensors (Fig. 19.2.4), which achieve 12% photon-detection probability (PDP) at 520nm (the peak emission of widely used green calcium indicators) with a median dark-count rate (DCR) of 26cps. We observed pile-up nonlinearities in the SPAD counts for high photon-flux regimes, for which we compensated by linearizing the sensor response in order to enhance image quality and extend dynamic range. The temporal response of the imager was evaluated by sweeping the delay between the turn-off time of the excitation µLED and the turn-on time of SPAD gating clocks while imaging Fluoresbrite YG 10µm-diameter beads. We achieved a peak signal-to-background ratio (SBR) of 26:1 and measured the beads lifetime to be ~6ns. The optical power density as a function of drive current for both blue and green µLEDs is characterized in order to find the operating points for imaging and stimulation at the 200µm cortex depth (Fig. 19.2.4).

Calibration of the lens-less imaging is performed by sweeping a 30µm-wide col/row line slit (to mimic a 520nm diffused fluorescent line source) in the X/Y direction, respectively, across the entire FoV [2]. In Fig. 19.2.5, the resolution is measured by imaging a double-line slit mask with 30µm width and 60µm spacing. The cross-section of the reconstructed double-line slit images shows better than 60µm lateral resolution. Even though the sensor is missing 12.5% of the pixels of a full 160×160 array due to the placement of µLEDs on the chip, the computational lens-less imaging is able to compensate for these "gaps" in image reconstruction which would not be possible in a lens-based system.

The chip consumes 40mW power in addition to 3mW and 2mW for excitation and optogenetics (1ms pulse-width at 20Hz) illumination, respectively. Measurements summary and comparison with prior fluorescence imagers are presented in Fig. 19.2.6. Finally, a sparse sample of 10µm-diameter beads on a glass cover slip is imaged with our device and a confocal microscope simultaneously. Figure 19.2.7 shows the results under ~0.5mW/mm² excitation intensity. The false-positive artifacts in the reconstructed image are caused by insufficient SBR which requires further improvements to the optical filtering.

We have demonstrated a mechanically flexible, low-power, implantable, and lens-less device for all-optical neural stimulation and recording that achieves better than 60µm resolution over 5.4×5.4mm² FoV. Our approach is the first step toward a fully implantable all-optical recording and stimulation brain interface device that can achieve better than cm² FoVs.

Acknowledgments:
We gratefully acknowledge TSMC for providing fabrication support for the SPADs employed here. This work was supported in part by DARPA under Contract N66001-17-C-4012 and by the National Science Foundation under Grant 1706207.

References:
[1] K. K. Ghosh et al., "Miniaturized integration of a fluorescence microscope," *Nature Methods*, vol. 8, pp. 871–878, Oct. 2011.
[2] J. K. Adams et al., "Single-Frame 3D Fluorescence Microscopy with Ultraminiature Lens-less FlatScope," *Science Advances*, vol. 3, no. 12, pp. 1-9, Dec. 2017.
[3] E. P. Papageorgiou et al., "Chip-scale fluorescence imager for in vivo microscopic cancer detection," *2017 Symposium on VLSI Circuits*, pp. C106-C107, June 2017.
[4] C. Lee et al., "An on-chip 72×60 angle-sensitive single photon image sensor array for lens-less time-resolved 3-D fluorescence lifetime imaging," *2014 Symposium on VLSI Circuits*, pp. 1-2, June 2014.
[5] C. Lee et al., "A 512-Pixel 3kHz-Frame-Rate Dual-Shank Lensless Filterless Single-Photon-Avalanche-Diode CMOS Neural Imaging Probe," *ISSCC*, pp. 198-200, Feb. 2019.

 978-1-7281-9549-0/21/$31.00

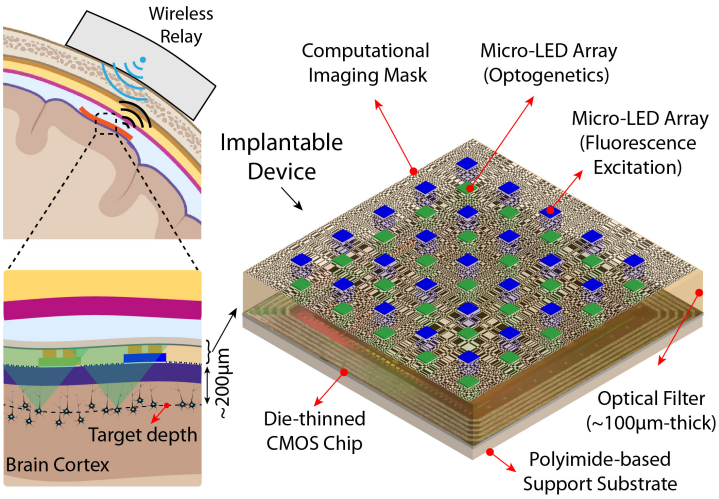

Figure 19.2.1: Proposed mechanically flexible, implantable device for all-optical neural recording and stimulation.

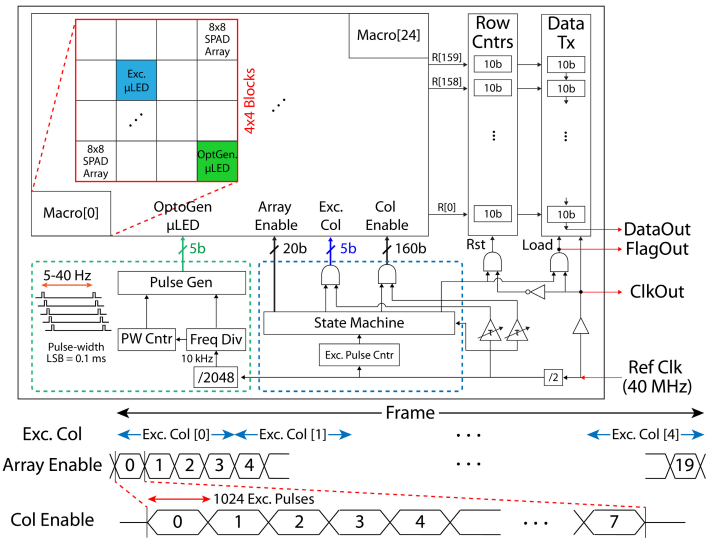

Figure 19.2.2: Block diagram of the neural interface chip with the timing diagrams of control signals for rolling-shutter imaging and stimulation included (all the control and enable signals are thermometer coded).

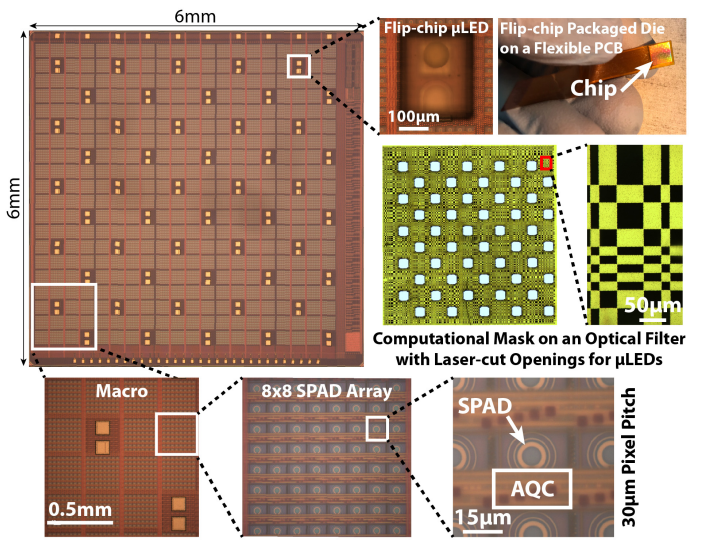

Figure 19.2.3: Micrographs of a bare die and imager's sub-blocks, a flip-chip bonded µLED, computational mask fabricated on the flexible optical filter, and a flip-chip packaged chip on a flexible PCB.

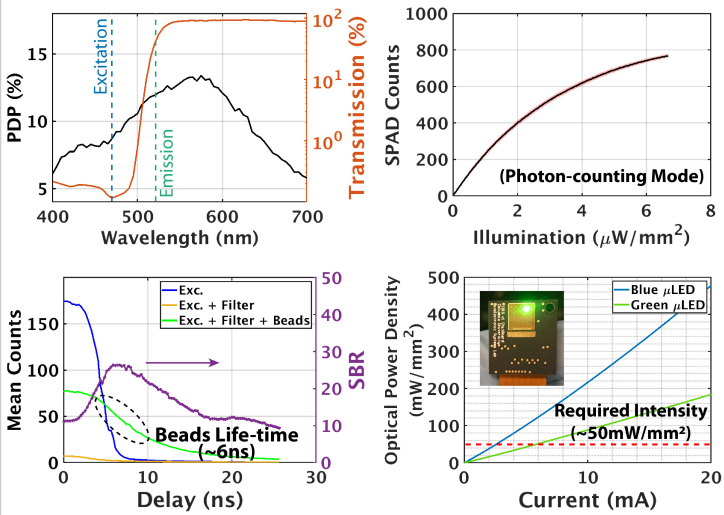

Figure 19.2.4: SPAD's PDP and filter transmission (top left), SPAD's non-linear response (top right), time-gating performance averaged over all pixels (bottom left), and µLEDs optical power density (bottom right).

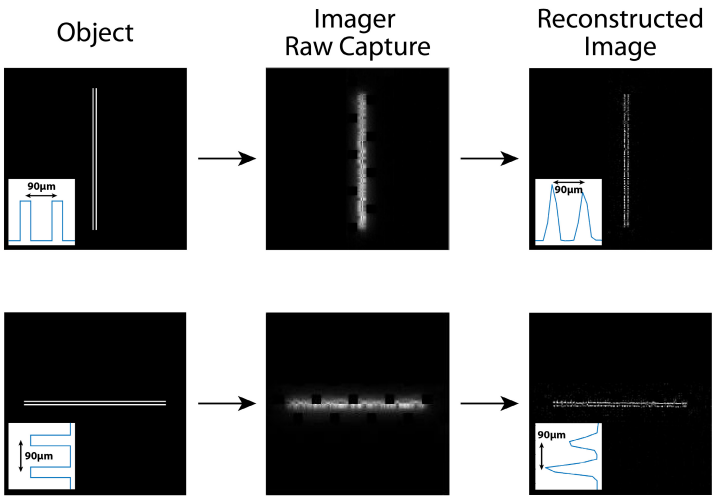

Figure 19.2.5: Imager's resolution characterization using vertical and horizontal double-line slits with 60µm spacing (90µm pitch) as a ground-truth (insets show median intensity across the lines).

Reference	VLSI' 17 [3]	VLSI' 14 [4]	**This Work**
CMOS Technology	0.18µm	0.18µm	0.13µm
Pixel Pitch (µm)	55	35	30
FF / PDP (%)	28 / 5* (QE)	14.4 / 2.7	5 / 12
Excitation / Emission Wavelength (nm)	450 / 705	385 / 540	470 / 520
Resolution (µm)	220	1000*	< 60
Field of View (mm²)	4.7x2.25	2.1x2.5	5.4x5.4
Frame-rate (fps)	20	N/R	125
Power (mW)**	3.5+	83.8	40
Array Size	80x36	72x60	160x160
Pixel's Photon Acceptance Angle FWHM (degree)	±18	±10	±70
Readout Data-rate (Mb/s)	N/A	N/R	40
Integrated Light Source	No	No	Yes

* Estimated from figures/data, ** Illumination power not included, + Not including off-chip ADCs

Figure 19.2.6: Performance summary and comparison to prior works.

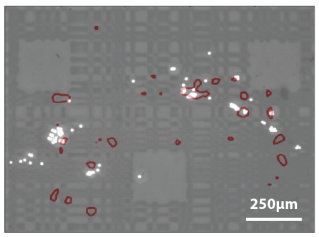

Confocal – Reconstruction Overlap

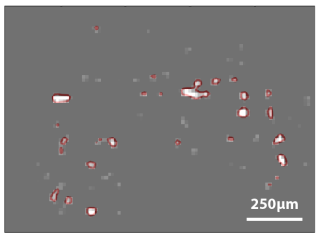

Reconstructed Chip Capture

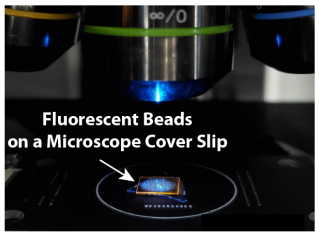

Fluorescence Imaging

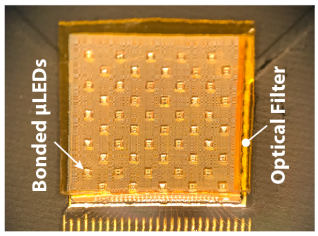

Chip with the Computational Mask

Figure 19.2.7: Imaging fluorescent beads with 10µm-diameter and comparison with confocal microscope's images. Reconstructed chip capture is normalized and red contours highlight the counts above half of the maximum.

978-1-7281-9549-0/21/$31.00 ©2021 IEEE